Low Energy, Non-Cortical, Graphene Nanoribbon-Based STDP Plastic Synapses

Laurenciu, Nicoleta Cucu; Timmermans, Charles; Cotofana, Sorin D.

DOI
10.1109/MNANO.2022.3208722

Publication date
2022

Document Version
Final published version

Published in
IEEE Nanotechnology Magazine

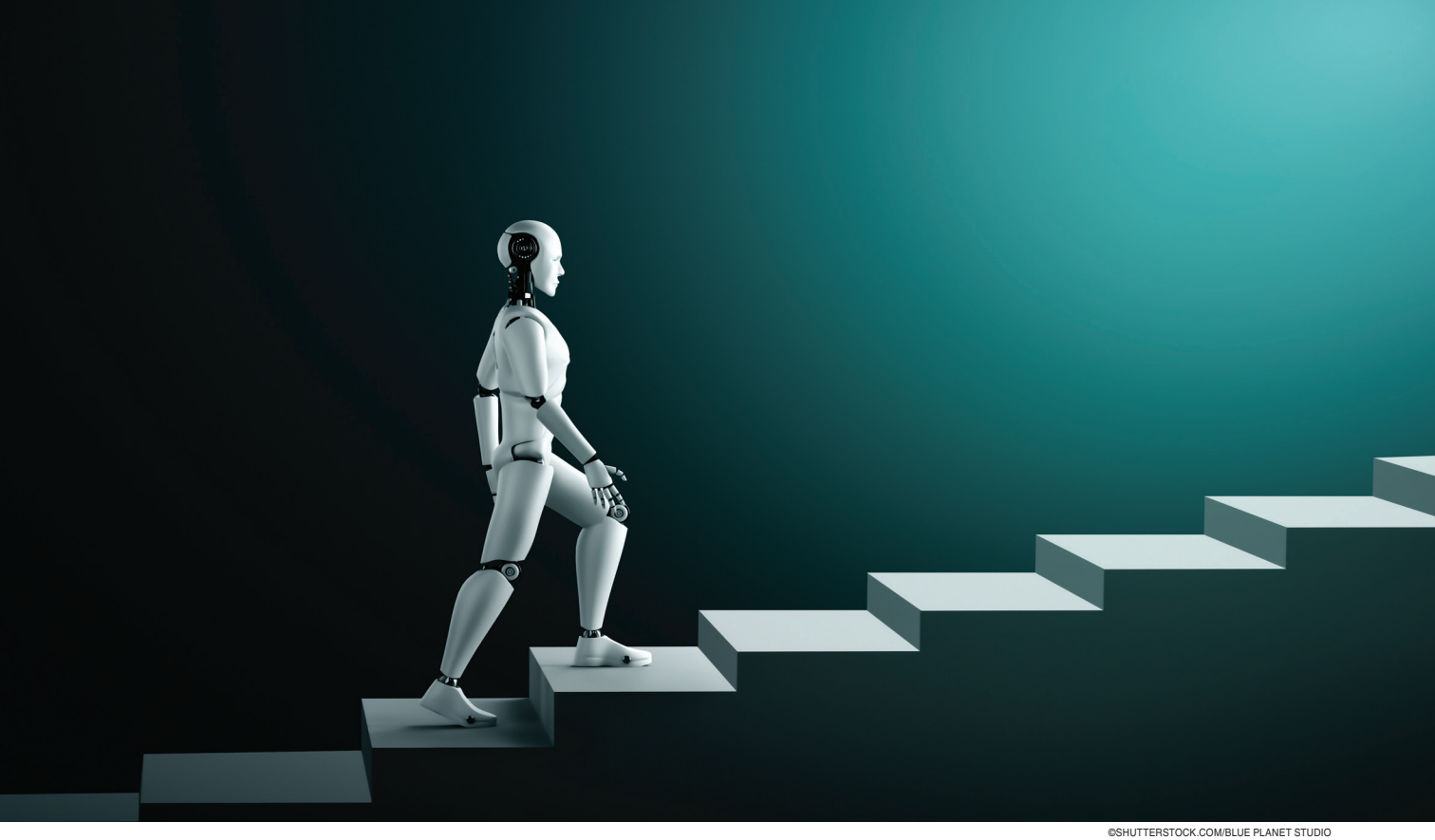

Low Energy, Non-Cortical, Graphene Nanoribbon-Based STDP Plastic Synapses

THE REALIZATION OF ENERGY efficient, low area, and fast processing neuron and synapse circuits is of prime importance for unleashing neuromorphic computing full potential. In this paper, we introduce a graphene-based synapse, which can emulate Spike Timing Dependent Plasticity (STDP) and Short/Long Term Plasticity (STP/LTP) with variable signal amplitude and temporal dynamics. The synapse operation is validated by means of SPICE simulations, and its synaptic modulation ability is showcased through reinforcement learning within a Spiking Neural Network for robotic navigation with obstacles avoidance. Besides its functional versatility, the proposed

Digital Object Identifier 10.1109/MNANO.2022.3208722
Date of current version: 20 January 2023

NICOLETA CUCU LAURENCIU, CHARLES TIMMERMANS, AND SORIN D. COTOFANA

1932-4510/23©2023IEEE

graphene-based synapse can potentially occupy low active area ($\approx 170\text{nm}^2$) and operate at low voltage (200mV). When compared with a biological brain synapse, its energy consumption per spike for a weight update operation (0.5fJ) is $20\times$ lower, while the processing speed is increased by six orders of magnitude. Such properties are essential desiderata for the realization of large scale neuromorphic systems, making the proposed graphene-based synapse an outstanding candidate for this purpose.

INTRODUCTION

Neuromorphic computing, which aims to carry out different data processing tasks while taking inspiration from the brain structure and operating principles that underlie its outstanding abilities (e.g., robustness in the presence of noise, energy effectiveness, massive parallel processing, suitability for complex tasks solving), has recently emerged as a very promising vista for future diverse and sustainable computing technologies. Spiking Neural Networks (SNNs) are of particular interest as they capture in a biologically plausible way the neural dynamics [1], [2], offering perspectives for brain-alike capabilities.

Synapses (schematically illustrated in Figure 1), which ensure signal processing and connectivity between neurons, are the most abundant neural components and are believed to play an essential role in human brain learning, hence, the impetus for efficient artificial synapse implementations. The preponderant state-of-the-art synapse implementations rely on CMOS technology and energy efficient CMOS synapses have been proposed in, e.g., [3], [4], [5], [6]. Nevertheless, they rely on a rather complex circuitry with many transistors, as CMOS devices cannot inherently mimic the analog synaptic behaviour. Furthermore, the CMOS technology is approaching atomic feature size, which brings power consumption and reliability concerns. Recently, emerging resistive switching memory devices, e.g., RRAM, STTRAM, phase-change memory [7], have enabled the road towards artificial synapses implementations, e.g., [8], [9], [10], [11], with simple structure (only one or a few resistive switching memory devices per synapse), synaptic functionality mimicked through inherently analog behavior, low energy consumption, and good scalability potential. However, they suffer from temporal and spatial variability of the resistive states, which may result in undesired stochasticity in neuromorphic systems. On the other hand, graphene, a 2D carbon atom honeycomb lattice material, emerged as a prominent post-Si frontrunner, due to its unique combination of excellent properties, e.g., ballistic transport, atomic thinness, inherently analog nature, biocompatibility [12], [13], [14], which taken together have not been seen in other materials thus far. Thus, graphene-based synapses with various plasticities were demonstrated at device level with bilayer graphene [15], [16]. In [15], the authors modulate the synaptic plasticity via external back gate voltage, while in [16], the device conductance is controlled by changing the concentration of the Lithium ions located between the graphene layers. While reporting low power switching ability and low variability, the obtained synaptic efficiency is small ($<0.01\%$ for [15], and $<2\%$ for [16]), which limits the synaptic modulation extent for learning.

In this paper, we propose a graphene-based synapse implementation, built from complementary arranged generic Graphene NanoRibbon (GNR) devices consisting of monolayer graphene on top of an insulating material, and with a doped substrate acting as back gate. The current flow in the device GNR channel is induced by a drain-to-source bias voltage and is modulated via external voltages applied on top and/or back gates. The synaptic plasticity functionality, i.e., Spike Timing Dependent Plasticity (STDP), Short Term Plasticity (STP), and Long Term Plasticity (LTP), is emulated via GNR devices with appropriately tailored topologies, while the plasticity temporal evolution is determined by the amount of interfacial charge traps. The proposed synapse is functionally versatile, as its output signal can exhibit various amplitudes and temporal dynamics associated with different synaptic receptors (AMPA, NMDA, GABA). The GNR-based synapse is validated by means of SPICE simulations, and its synaptic modulation ability is demonstrated in a practical scenario: robotic navigation with obstacle avoidance within a confined environment. To this end, we propose a Spiking Neural Network (SNN) that can infer the robot's course of action when faced with obstacles, utilize instances of the proposed synapse and graphene-based leaky integrate and fire neurons [17] to implement it, and demonstrate its ability to quickly identify the proper trajectory to target by means of reinforcement learning. Besides functional flexibility, the proposes synapse potentially requires a small real estate ($\approx 170\text{nm}^2$), operates at low supply voltage (200mV), and exhibits an energy consumption of 0.5fJ per synaptic event, which amounts to $\approx 20\times$ less energy consumption when compared to a brain synapse. Furthermore, it operates at ns time-scale, enabling six orders of magnitude processing speed-up relative to a brain synapse. All these properties are very attractive for

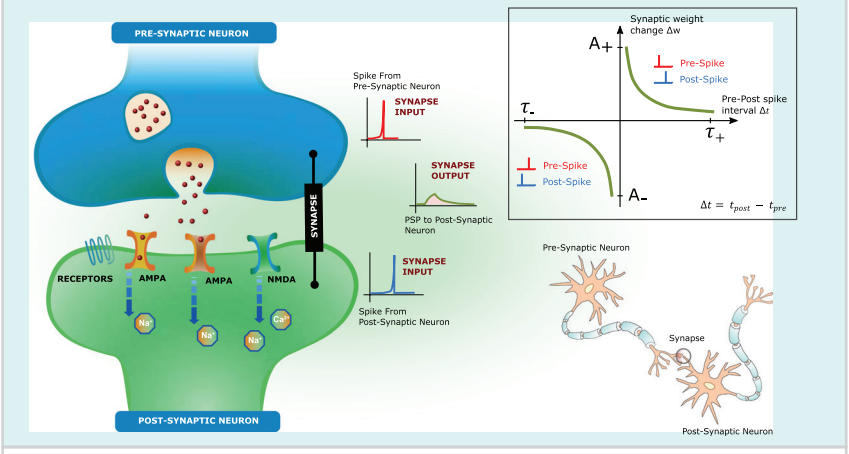

FIGURE 1 Simplified synapse illustration and Spike Timing Dependent Plasticity (STDP) principle for synaptic modulation.

neuromorphic computation in large scale scenarios, suggesting that the proposed GNR-based synapse can be a highly potent candidate to these ends.

The remaining of this paper is structured as follows: The "Background" section presents underlying synaptic plasticity concepts and the generic graphene-based device. In the "GNR-Based Synapse With STDP Plasticity" section, we introduce the proposed GNR-based synapse circuitry and describe its basic operation. In the "Robot Navigation Case Study" section, we consider a robotic navigation with obstacle avoidance application, and we introduce an SNN implementation that makes use of the proposed synapse in conjunction with graphene-based leaky integrate and fire neurons able to quickly identify proper robot trajectory by means of reinforcement learning. In the "Conclusion" section, we summarize the main findings of the paper.

BACKGROUND

In this section, we outline the underlying concepts of synaptic plasticity and describe the generic graphene-based device we utilize into the proposed synapse implementation.

SYNAPSES AND STDP PLASTICITY

Synapses are communication sites where neuron pairs pass signals among themselves. Besides being merely transmission media, synapses also serve a processing role, as they can strengthen or weaken the transmitted signals via the synaptic plasticity mechanism. As illustrated in Figure 1, a synapse has two inputs (i.e., a pre-synaptic spike coming from the pre-synaptic neuron and a post-synaptic spike coming from the post-synaptic neuron) and one output (i.e., a Post-Synaptic Potential (PSP), which travels to the post-synaptic neuron. In biological neurons, glutamate, the neurotransmitter released into the synapse from the pre-synaptic neuron, can bind to various receptors types (e.g., GABA, NMDA, AMPA) on the post-synaptic neuron [18]. These receptors are coupled with ion channels that can modulate the post-synaptic neuron excitability, by gating the influx of Calcium and Sodium ions. For instance, the AMPA receptor is coupled with an ion channel that lets Sodium ions enter the post-synaptic neuron, when the glutamate from the pre-synaptic neuron binds to it. As a result of the Sodium influx, the post-synaptic cell becomes depolarized, and when this depolarization reaches a certain threshold, a nerve impulse (a spike) is generated and transmitted. While for the pre and post spikes (the synapse inputs) the information is encoded in frequency, for PSP (the synapse output), the information is encoded in amplitude. Thus, a synapse ensures PSP amplitude modulation as a function of input spikes frequency rates, which is process known as synaptic plasticity. The most common type of synaptic plasticity is Spike Time Dependent Plasticity (STDP). STDP can be regarded as a learning process during which PSP amplitude (i.e., the strength of the connections between two neurons, also known as synaptic weight) is updated based on temporal correlations between pre- and post-synaptic spikes [1]. Specifically, if a pre-synaptic spike precedes a post-synaptic spike, then the synaptic weight is potentiated (PSP amplitude increases). Conversely, if a post-synaptic spike occurs before a pre-synaptic spike, then the synaptic weight is depressed (PSP amplitude decreases).

Formally, the synaptic weight (PSP amplitude) increase/decrease Δw can be expressed as [1]:

$$\Delta w(\Delta t) = \begin{cases} A_+ \cdot e^{-\Delta t/\tau_+} & \Delta t > 0 \quad \text{(potentiation)} \\ 0 & \Delta t = 0 \\ A_- \cdot e^{-\Delta t/\tau_-} & \Delta t < 0 \quad \text{(depression)} \end{cases} \quad (1)$$

where $\Delta t = t_{post} - t_{pre}$ is the temporal difference between the post- and the pre-synaptic spikes, τ_+ and τ_- are the time decaying constants for the weight update potentiation and depression, and A_+ and A_- control the magnitude range of the weight update for potentiation and depression, respectively.

The PSP amplitude W is then updated at every spike occurrence (whether it is post or pre spike), as

$$W = W + \Delta w(\Delta t)$$
$$\Delta t = t_{post} - t_{pre} \quad (2)$$

While the amplitude of the PSP signal is influenced by both pre and post spikes occurrences, the actual PSP signal is elicited by pre spikes only.

GENERIC GNR-BASED DEVICES

The fundamental building unit for synapses implementation is the graphene-based device illustrated in Figure 2. The device includes a Graphene NanoRibbon (GNR) sheet that serves as a conduction channel when exposed to a drain-to-source bias voltage $V_d - V_s$. The nanoribbon geometry and its contacts topology determine the GNR device conduction profile, while the actual conductance value is modulated by means of external voltages exerted via top and/or back

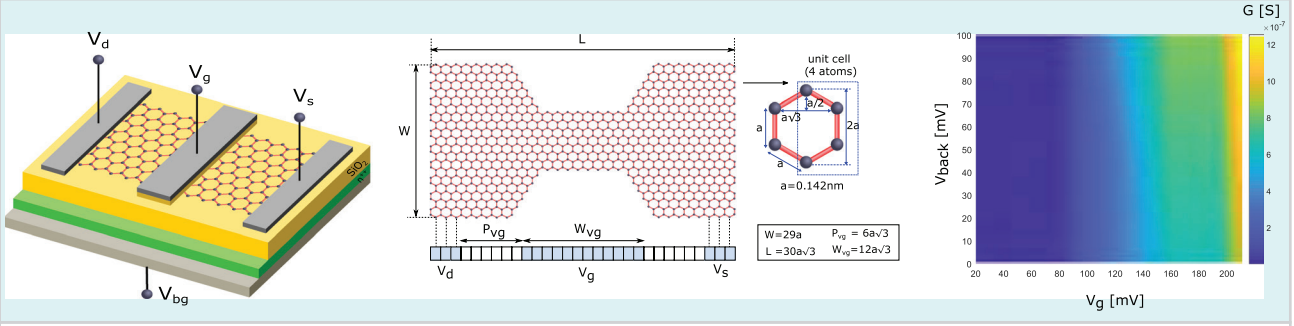

FIGURE 2 Generic graphene-based device and conductance map example.

gates [19]. Figure 2 presents a GNR topology example and its conductance map obtained under constant $V_d - V_s$ while sweeping the top gate and the back gate voltages. As different GNR conductance maps induce different electrical functionalities, such graphene-based devices have been utilized for Boolean logic gate implementations, as well as other non-Boolean logic circuits [20], [21], [22], [23]. Furthermore, it has been experimentally observed that graphene-based devices inherently exhibit interface traps, which can trap and release GNR carriers [12]. Such traps are responsible for inducing a hysteretic I-V behaviour, which can be naturally exploited for synaptic plasticity (e.g., for emulating the synapse output signal magnitude dependence on the synapse's accrued past activities [24]).

GNR-BASED SYNAPSE WITH STDP PLASTICITY

A practical way to implement in hardware the amplitude modulation for the STDP rule (Equations (1) and (2)) [25] is conceptually exemplified in Figure 3.

It makes use of two separate traces: (i) a pre trace left behind only by pre spikes—the pre trace is updated by the fixed amount A_+ at every pre spike arrival time moment, after which it decays exponentially in the absence of any pre spikes—and (ii) a post trace left only by post spikes—the post trace is updated by the fixed amount A_- at the every post spike arrival time moment, and it decays exponentially in the absence of subsequent post spikes. As concerns the weight update, at the arrival moment of a post spike, Δw is increased proportionally to the momentary value of the pre trace (potentiation caused by pre before post spikes). Analogously, at the arrival moment of a pre spike, Δw is decreased proportionally to the momentary value of the post trace (depression induced by post before pre spikes). The amplitude increase/decrease Δw is then used to modulate a fixed amplitude PSP signal and, thus, yields the synaptic output signal. We adopt the same rationale for the design of the proposed GNR synapse.

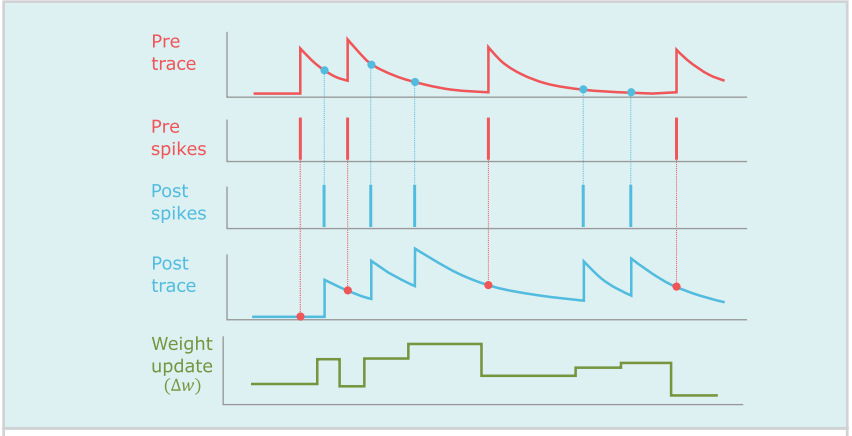

FIGURE 3 Synaptic weight increment/decrement (Δw) derivation via STDP rule.

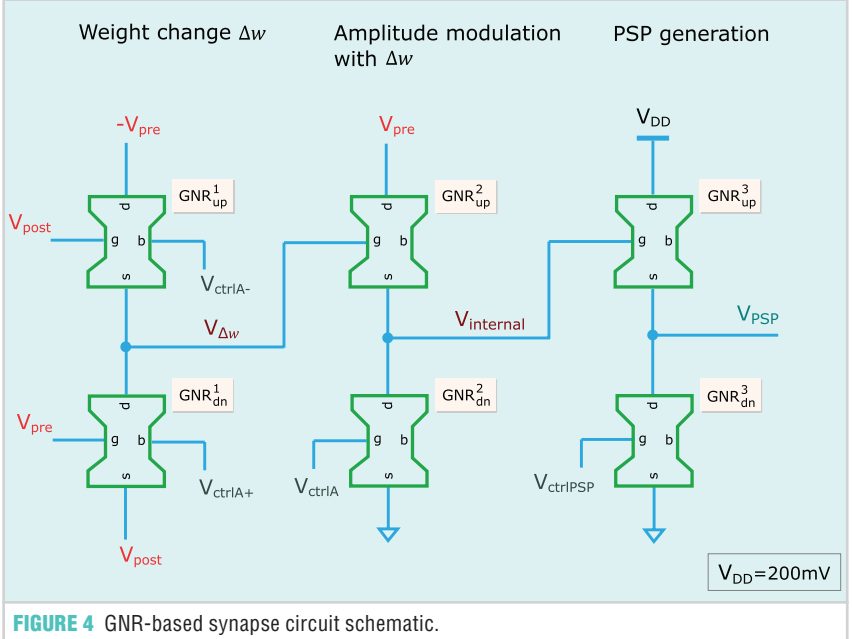

FIGURE 4 GNR-based synapse circuit schematic.

Figures 4 and 5 illustrate the GNR synapse circuit schematic, and its basic operating principle, respectively. The GNR synapse, functionally speaking, consists of three blocks: (i) the synaptic weight change block, that computes the PSP amplitude increase/decrease Δw, based on the timing difference between pre and post spikes according to the STDP rule, (ii) the PSP amplitude modulation block, that determines the PSP total amplitude by enacting the Δw amplitude increase or decrease for every pre spike event, and (iii) the PSP signal generation block, which elicits a PSP signal every time a pre spike occurs. The synapse circuit in Figure 4 has as inputs the pre- and post- synaptic spike signals, denoted by V_{pre} and V_{post}, and generates as output the PSP signal V_{PSP} via its three comprising blocks as follows:

- The weight change block (GNR^1_{up} and GNR^1_{dn}). GNR^1_{up} generates the trace left by the post spikes and samples this trace everytime a pre spike occurs. The sampled values are further reflected proportionally in the weight change $V_{\Delta w}$ decrease. Similarly, GNR^1_{dn} converts the pre spikes into a pre trace that is sampled by post spikes. As a result, a proportional increase of weight change $V_{\Delta w}$ is induced. As illustrated in Figure 5, $V_{\Delta w}$ increase is smaller than its decrease, due to smaller

V_{pre} trace sampled values in the former case.

- The PSP amplitude modulation block (GNR^2_{up} and GNR^2_{dn}). This block modulates the amplitude of every pre spike with the variation amount given by the weight change $V_{\Delta w}$. Figure 5 displays the amplitude modulated V_{pre} signal $V_{amplitude}$ with amplitude decrements, i.e., zoomed-in peaks, consistent with the weight change $V_{\Delta w}$.
- The PSP signal generation block (GNR^3_{up} and GNR^3_{dn}). The synapse output signal V_{PSP} with amplitude proportional to the $V_{amplitude}$ signal and exponential temporal dynamics is finally generated. For the example considered in Figure 5, a zoom on V_{PSP} peak values reveals depression dynamics, in line with the expectations for the post-before-pre spike pairings case.

Figure 6 depicts the GNR topologies of the proposed graphene-based synapse devices, which we identified by means of an atomistic model based Design Space Exploration (DSE) process. Concerning the interface trap profile for the atomistic-level graphene-based device modelling, we assumed an interface trap density of $2.363 \cdot 10^{13} cm^{-2}(eV)^{-1}$ and a trapping/detrapping time constant of 1.6ms [26], [27]. Note that to get proper synaptic behavior, each device has to deliver a certain functionality, i.e., conduction map, but more topologies can provide the same conduction map; thus, other than the GNRs in Figure 6 may also be appropriate.

SYNAPTIC ADAPTATION

The dynamics governing timing dependent synaptic plasticity may vary considerably across synapse types and brain regions [34]. Such diversity is believed to be reconciled though a variety of underlying modulatory mechanisms, among which the variation of the PSP amplitude (though STDP adaptation dynamics in particular) and of the overall PSP temporal dynamics are considered key adaptation determinants [35].

To control the PSP amplitude variation Δw, four control parameters, i.e., A_+, A_-, τ_+, and τ_- (as defined in Equation (1)), are typically employed for pair-wise STDP. The amplitude variation Δw specified by the STDP rule is an exponential function, and so, $A_{+/-}$ controls the amplitude of the exponential, while $\tau_{+/-}$ controls the exponential decay. For proposed GNR-based synapse, A_+ and A_- can be adjusted separately via the back-gate voltages of GNR^1_{up} and GNR^1_{dn}, respectively, denoted in Figure 4 as V_{ctrlA+} and V_{ctrlA-}. A coarse grain control common to both A_+ and A_- is possible as well by applying a top gate voltage V_{ctrlA} to GNR^2_{dn}. Figure 7(a) exemplifies the GNR-based synapse STDP weight change for three different A_+ and A_- settings. The time constants τ_+ and τ_- are kept constant in all three cases. The decaying behaviour of Δw for the proposed GNR-based synapse is induced by the trapping/de-trapping phenomena manifested by top-gate oxide defects [12], [24]. Figure 7(b) exemplifies the GNR-based synapse STDP weight change for three different τ_+ and τ_- settings, while keeping A_+ and A_- constant.

PSP signals can be either excitatory (positive PSP) or inhibitory (negative PSP), depending on the neurotransmitters binding to synaptic receptors. Since different types of synaptic receptors are responsible for different temporal dynamics of the PSP signal, the ability to modulate the PSP behaviour is essential. Figure 7(c) displays the PSP signals generated by proposed GNR-based synapse, for various temporal dynamics which correspond to different types of receptors: AMPA and NMDA (excitatory), $GABA_A$ and $GABA_B$ (inhibitory). The temporal dynamics afferent to each of the four PSP curves are induced by the GNR^3_{up} trapping/de-trapping phenomena, by

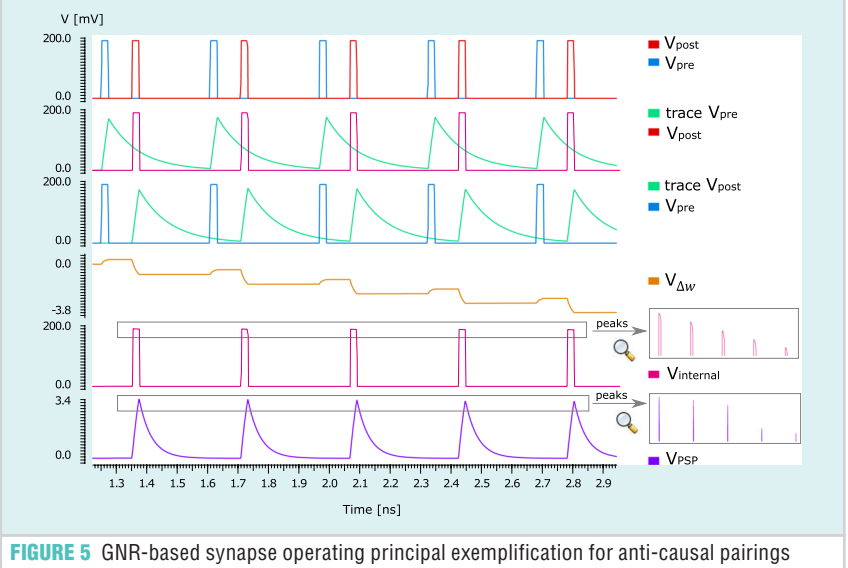

FIGURE 5 GNR-based synapse operating principal exemplification for anti-causal pairings of post-pre spikes (for inducing LTD).

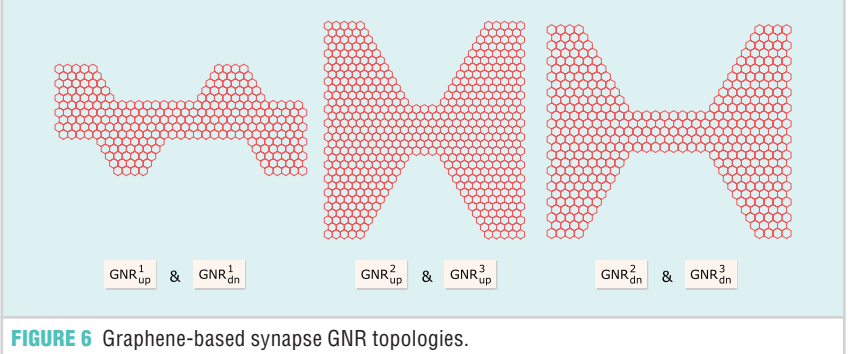

FIGURE 6 Graphene-based synapse GNR topologies.

considering different trapping/de-trapping time constant values.

AREA AND ENERGY EVALUATION

To have a better view on the synapse implementations landscape and the potential of proposed graphene-based synapse for energy efficient, low area neuromorphic systems, we evaluate comparatively in Table 1 the figures for state-of-the-art artificial synapses implemented in different technologies, e.g., CMOS, memristor, ferroelectric tunneling junctions, graphene.

As transpires from Table 1, from the area point of view, compared to CMOS implementations, the emergent technologies lend themselves to more compact implementations, which makes them better suited for high density of integration associated with large scale neuromorphic systems. From the energy consumption standpoint, there are designs which target the biologically plausible time-scale (ms), while other state-of-the-art synapse implementations target fast non-cortical processing, and operate on orders of magnitude higher frequency with a much lower energy envelope when compared to the brain synapse energy.

The proposed GNR-based synapse requires $\approx 170\text{nm}^2$ active area, operates at low voltage (200mV) and has an energy expenditure of ≈ 0.5 fJ per synaptic event (plasticity modulation and spike transmission) for ns timescale. Thus, accelerated computing with a speed-up factor of six orders of magnitude can be achieved by using the proposed GNR-based synapse. In addition, the energy savings $20\times$ smaller relative to the brain synapse, and the small real-estate requirements ($\approx 170\text{nm}^2$), are indicative of desired characteristics for large scale neuromorphic systems. Functionality-wise, the proposed GNR-based synapse can emulate STDP synaptic plasticity, which, depending on the synaptic

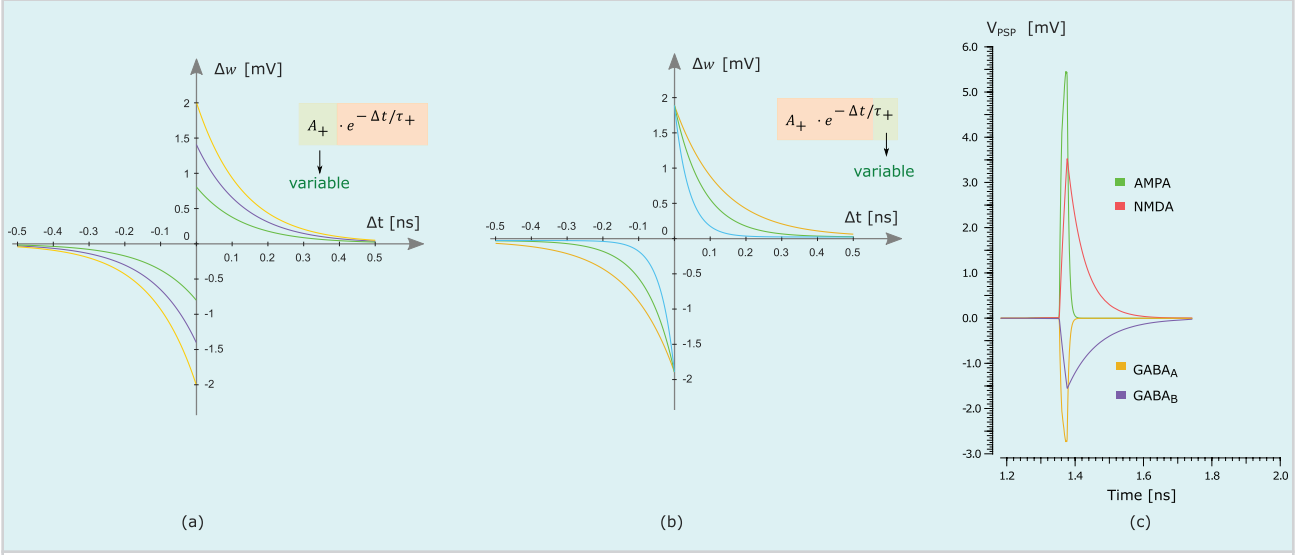

FIGURE 7 Synaptic adaptation of GNR-based synapse. (a), (b) PSP amplitude via STDP dynamics. (c) PSP temporal dynamics.

TABLE 1 Area and energy consumption for proposed and state-of-the-art artificial synapses

	PLASTICITY	TECHNOLOGY	OPERATION VOLTAGE	AREA	ENERGY/SPIKE	SPIKE TIMESCALE
Brain synapse	-	-	Spike: [–40,70] mV	-	10 fJ	ms
2020 [28]	STDP	CMOS 65nm	1.2 V	-	1…50 fJ	μs
2015 [29]	STP, LTP	CMOS 28nm	1 V	13 μm^2	2.3…30 nJ	10 μs . . . 1 ms
2020 [30]	STP, LTP, SRDP	Memristor	1 V	-	-	20 μs
2017 [31]	SRDP, STDP	Memristor	3 V	0.01 μm^2	-	μs . . . ms
2020 [32]	LTP	PCM	2.5 V	-	5…30 pJ	ns
2020 [33]	STP, LTP, STDP	FTJ	1.8 V	-	0.2…146 fJ	50 ns
2018 [16]	LTP, STDP	Graphene	100 mV	900 nm^2	40 aJ . . . 500 fJ	100 ns . . . ms
Proposed	STP, LTP, STDP	Graphene	200 mV	170 nm^2	0.5 fJ	ns

STDP - Spike Timing Dependent Plasticity; LTP - Long Term Plasticity; STP - Short Term Plasticity; SRDP - Spike Rate Dependent Plasticity PCM - Phase Change Memory; FTJ - Ferroelectric Tunneling Junction

retention time period, can lead to either short-term or long-term plasticity. The proposed design also features a rich set of STDP adaptations via external control voltages, resulting in various PSP amplitude and temporal dynamics. Such versatility makes the proposed GNR-based synapse particularly attractive for functionally diverse neuromorphic platforms.

ROBOT NAVIGATION CASE STUDY

To demonstrate the ability of our proposal to deliver proper synaptic plasticity, we assume as the discussion vehicle, a simple case of robot navigation towards a target within a confined environment with obstacles that shouldn't be collided with. The environment under consideration is a 500×500 pixel planar area inside which polygonal obstacles are randomly placed. As illustrated in Figure 8, the moving vehicle is a 2-wheel differential drive robot with 30×30 pixels area. As concerns the odometric ability, the robot is endowed with (i) a compass that measures its orientation relative to the Earth magnetic North and (ii) five ultrasonic sensors oriented towards robot's front, front left, left, front right, and right directions, that can sense the proximity of objects (environment walls, obstacles, target) within a distance range of 45 pixels. Additionally, we assume that the distance and orientation towards the target are known at all times. The robot can move 10 pixels towards the target, or relative to its own orientation 10 pixels to its left or right, and 20 pixels backwards. Starting from an initial position, the robot's goal is to reach the target position while avoiding obstacles. A co-simulation setup was employed for this context, and the spiking neural network was simulated by means of SPICE in Cadence, while the remaining simulation environment was written in C. For the GNR-based devices, the electronic transport properties are calculated using the atomistic level Tight-Binding Hamiltonian in order to capture the atomic interactions and the external potentials, the Non-equilibrium Green Function (NEGF) for solving the Schrödinger equation, and the Landauer-Büttiker formalism to derive the GNR current and conductance [36], [37]. Solving self-consistently a 3D Poisson equation yields the potential distribution on the graphene sheet, and computing the equivalent voltage shift of the trapped/detrapped charges at the graphene interface with the top gate oxide accounts for the hysteresis inducing phenomena [24]. To enable physical-level accurate and time effective simulation, a Verilog-A model is employed, with look-up tables containing extensive GNR conduction simulation data derived with the aforementioned methodology.

The robot can move 10 pixels towards the target, or relative to its own orientation 10 pixels to its left or right, and 20 pixels backwards.

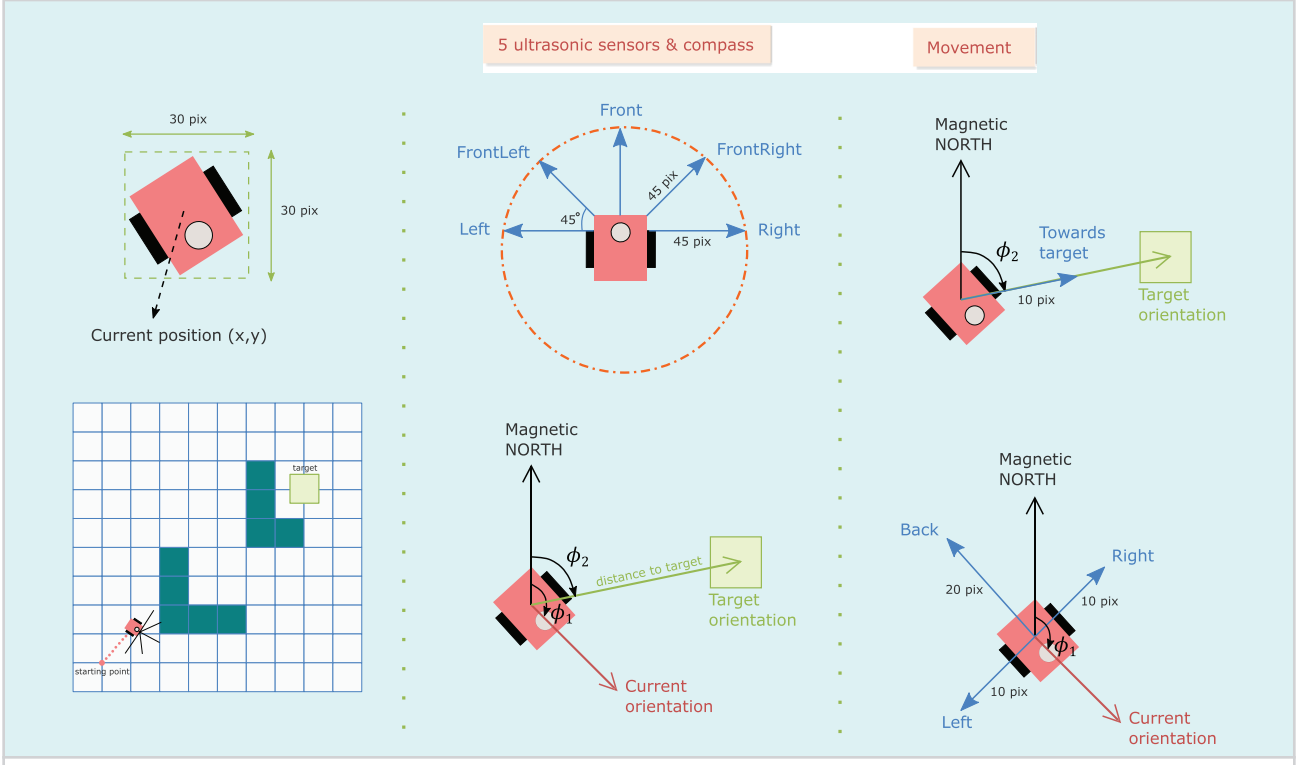

FIGURE 8 Navigational environment and robot's odometry and movement.

KINEMATICS

The robot's state at a given time moment t, $p(t)$, can be described by its center mass Cartesian coordinates (x, y) and orientation θ with respect to magnetic North, as $p(t) = [x \quad y \quad \theta]^T$. The kinematics of the 2 wheel differential-drive mobile robot, that describe the state transition between two consecutive time moments $(p(t+1) = p(t) + \dot{p})$, is expressed in the Cartesian coordinates as

$$\dot{p} = \begin{bmatrix} \dot{x} \\ \dot{y} \\ \dot{\theta} \end{bmatrix} = \begin{bmatrix} \cos(\theta) & 0 \\ \sin(\theta) & 0 \\ 0 & 1 \end{bmatrix} \cdot \begin{bmatrix} v \\ \omega \end{bmatrix} \quad (3)$$

The robot's linear and angular velocities, v and ω, respectively, are given by

$$\begin{bmatrix} v \\ \omega \end{bmatrix} = \begin{bmatrix} \frac{r}{2} & \frac{r}{2} \\ \frac{r}{L} & -\frac{r}{L} \end{bmatrix} \cdot [\omega_R \quad \omega_L] \quad (4)$$

where ω_L and ω_R are the angular left and right wheel velocities, L is the distance between the wheels, and r is the wheel radius.

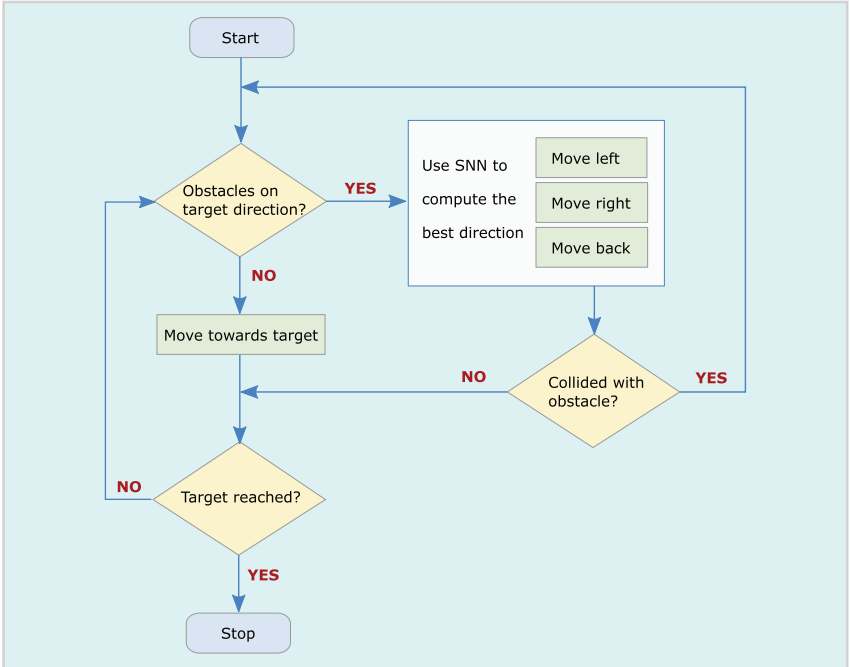

FIGURE 9 Robot navigational flow.

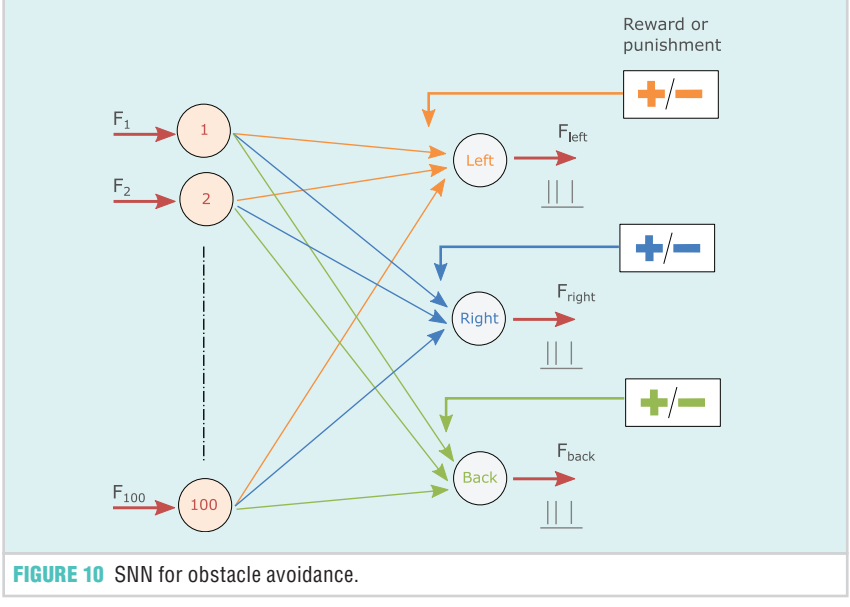

FIGURE 10 SNN for obstacle avoidance.

NAVIGATION STRATEGY

Figure 9 illustrates the block scheme of the robot navigational flow, where the obstacle avoidance navigational actions are inferred by a spiking neural network within a reinforcement learning approach.

From the initial position, the robot first rotates itself towards the target. The ultrasonic sensor readings are processed, and while they indicate no obstacle proximity within 45 pixels, the robot repeatedly moves 10 pixels towards the target. Otherwise, if an obstacle is detected by the sensors, the SNN is activated to compute the best course of movement in order to avoid the obstacle, i.e., move 10 pixels to either left or right, or 20 pixels backwards. When moving in the direction inferred by the SNN, if the robot has successfully avoided the obstacle, a reward is applied to the SNN, i.e., the synaptic pathways that lead to the successful obstacle avoidance direction are potentiated. In the case of colliding with the obstacle, a penalty is applied to the SNN to depress the synaptic connections that lead to the erroneous SNN movement direction output, and thus discourage such SNN outcome in the future. Upon obstacle collision, the robot position and orientation are reset to their initial values for a new trial. After a certain number of trials, the SNN learns the directions that lead to obstacles avoidance and the target is finally reached.

SNN REINFORCEMENT LEARNING

Reinforcement learning promotes the ability to select actions in response to the contingencies provided by the environment to one's subjective benefit. It is a meaningful learning paradigm for robotic navigation scenarios, as when operating in environments about which complete knowledge is unattainable, the robot's correct action for each state is not known, but rather, it has to be inferred through trial-and-error interaction with the environment, i.e., from post factum rewards and punishments. Recently, neuroscience studies have shown that certain decision

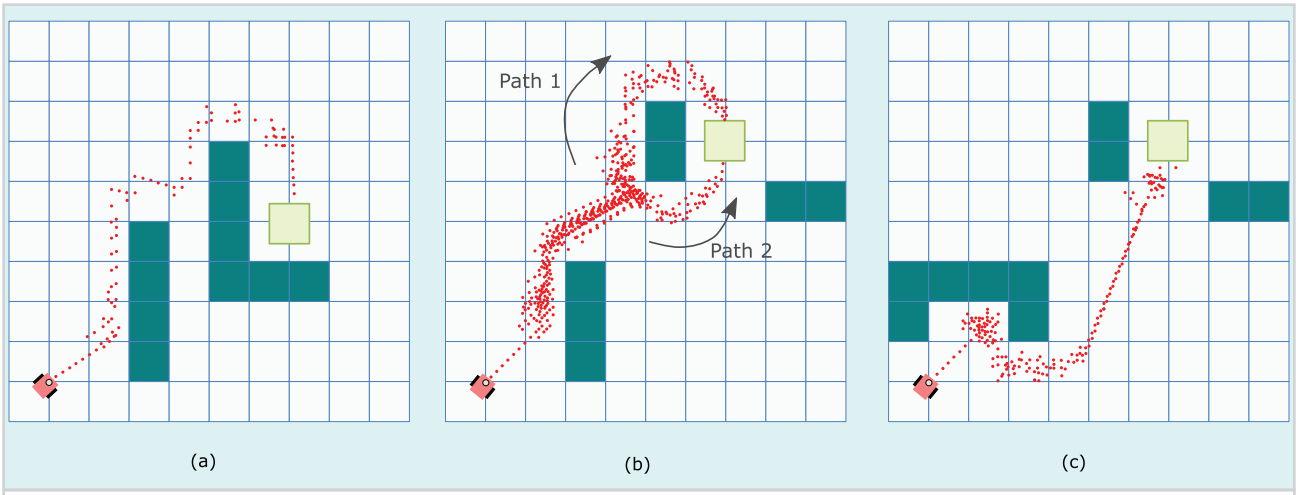

FIGURE 11 SNN reinforcement learning generated robot traces.

making processes in the brain rely on some form of reinforcement based on reward [38]. One hypothesis is that the reward is conveyed via dopamine neurons, and can modulate the synapses STDP plasticity [39], [40]. For the robotic navigation task, we employ an SNN and reinforcement learning to infer the obstacle avoidance action given the current robot state. The SNN as illustrated in Figure 10, has two layers of graphene-based leaky integrate and fire neurons [17] (1^{st} layer which encodes the robot's state space (x, y, θ), and 2^{nd} layer which encodes the action space (move left, move right, move backwards)), and an extra layer of dopaminergic neurons [41]. To relay the robot state information to the SNN, the 500×500 pixels environment is quantized into 100 50×50 pixels cells. Each such cell j corresponds to one L_1 neuron, which receives as input a spike train with an inhomogeneous Poisson process firing rate F_j given by

$$F_j = F \cdot exp\left(-\frac{(d - d_j)^2}{c^2}\right) \quad (5)$$

where d is the robot's distance to target, d_j is the cell j center point distance to target, and F and c are design constants [42]. The SNN output neuron with the highest firing rate will determine the robot's next movement direction in order to avoid the obstacle. A reward or punishment is further applied depending on successful obstacle avoidance as a result of the SNN inferred action.

Figure 11 presents the environment configurations we utilized for evaluating the SNN synaptic modulation ability for obstacle avoidance learning and the obtained robot trajectories. For every environment, multiple trials are repeated, and the number of collisions is recorded. A trial resets the obstacle pose to the initial position and ends when a collision with an obstacle occurs or when the target is reached. In the the environment with two obstacles in Figure 11(a), the robot collided four times across four trials until the target is first reached. Its four navigation paths across the trials are depicted in red. After first reaching the target, subsequent navigation trials are collisionless. Figure 11(b) illustrates an environment where the robot has 0.5 probability to go left or right when detecting the second obstacle and the SNN managed successfully learn the two possible paths to the destination. The two paths lengths however are not equal, so it might be advantageous to prime the robot's reaction towards the shorter 2^{nd} path, which can be potentially achieved by applying a reward at the end of each trial for which the target was reached via path 2. In this way, the robot will eventually learn to follow path 2 only, but we did not follow this avenue however, as navigation strategy optimization (e.g., distance minimization) is outside the scope of this paper. For this environment, the robot required 14 trials to first reach the target. Figure 11(c) environment has a more complex obstacle setup with a concavity where the robot can get stuck, but despite this the robot first reaches the target after 10 trials. Our simulations indicate that collision avoidance behavior performance improved across trials, which clearly demonstrate that the proposed GNR-based synapse can be successfully utilized for SNN implementations.

CONCLUSION

In this paper, we propose a generic GNR-based synapse able to emulate Spike Timing Dependent Plasticity (STDP) and provide Post-Synaptic Potential (PSP) amplitude and temporal dynamics associated with different synaptic receptors (AMPA, NMDA, GABA). Besides functional versatility, the proposed GNR-based synapse can potentially necessitate small active area ($\approx 170 nm^2$), operate at low supply voltage ($200 mV$), and has low energy consumption ($0.5 fJ$) when operating in the ns non-cortical, fast processing mode. With respect to a biological synapse, the GNR-based synapse can enable six orders of magnitude faster processing, while consuming $20\times$ less energy. All these characteristics are highly desirable for neuromorphic systems with high density of integration. We validated the synapse operation by means of SPICE simulations in Cadence and demonstrated its synaptic plasticity abilities by implementing a Spiking Neural Network (SNN) with reinforcement learning capabilities for obstacle avoidance robotic maneuvering within a confined space.

ABOUT THE AUTHORS

Nicoleta Cucu Laurenciu (n.cuculaurenciu@science.ru.nl) is with the High Energy Physics Department, IMAPP, Radboud University, 6525, AJ, Nijmegen, the Netherlands.

Charles Timmermans (c.timmermans@science.ru.nl) is with the High Energy Physics Department, IMAPP, Radboud University, 6525, AJ, Nijmegen, the Netherlands.

Sorin D. Cotofana (s.d.cotofana@tudelft.nl) is with the Department of Quantum and Computer Engineering, Delft University of Technology, 2628, CD, Delft, the Netherlands.

REFERENCES

[1] W. Gerstner, W. M. Kistler, R. Naud, and L. Paninski, *Neuronal Dynamics: From Single Neurons to Networks and Models of Cognition*. Cambridge, U.K.: Cambridge Univ. Press, 2014.

[2] H. Paugam-Moisy and S. M. Bohte, "Computing with spiking neuron networks," in *Handbook of Natural Computer*, vol. 1. Berlin, Heidelberg, Germany: Springer, 2012, pp. 1–47, doi: 10.1007/978-3-540-92910-9_10.

[3] S. B. Furber et al., "Overview of the spinnaker system architecture," *IEEE Trans. Comput.*, vol. 62, no. 12, pp. 2454–2467, Dec. 2013, doi: 10.1109/TC.2012.142.

[4] P. A. Merolla et al., "A million spiking-neuron integrated circuit with a scalable communication network and interface," *Science*, vol. 345, no. 6197, pp. 668–673, 2014, doi: 10.1126/science.1254642.

[5] B. V. Benjamin et al., "Neurogrid: A mixed-analog-digital multichip system for large-scale neural simulations," *Proc. IEEE*, vol. 102, no. 5, pp. 699–716, May 2014, doi: 10.1109/JPROC.2014.2313565.

[6] J. Schemmel, D. Briiderle, A. Griibl, M. Hock, K. Meier, and S. Millner, "A wafer-scale neuromorphic hardware system for large-scale neural modelling," in *Proc. IEEE Int. Symp. Circuits Syst.*, 2010, pp. 1947–1950, doi: 10.1109/ISCAS.2010.5536970.

[7] D. B. Strukov, G. S. Snider, D. R. Stewart, and R. S. Williams, "The missing memristor found," *Nature*, vol. 453, no. 7191, 2008, Art. no. 80, doi: 10.1038/nature06932.

[8] N. Du et al., "Synaptic plasticity in memristive artificial synapses and their robustness against noisy inputs," *Front. Neurosci.*, vol. 15, pp. 1–14, 2021 doi: 10.3389/fnins.2021.660894.

[9] S. Saïghi et al., "Plasticity in memristive devices for spiking neural networks," *Front. Neurosci.*, vol. 9, 2015, Art. no. 51, doi: 10.3389/fnins.2015.00051.

[10] Y. Babacan and F. Kaçar, "Memristor emulator with spike-timing-dependent-plasticity," *AEU-Int. J. Electron. Commun.*, vol. 73, pp. 16–22, 2017, doi: 10.1016/j.aeue.2016.12.025.

[11] S. H. Jo, T. Chang, I. Ebong, B. B. Bhadviya, P. Mazumder, and W. Lu, "Nanoscale memristor device as synapse in neuromorphic systems," *Nano Lett.*, vol. 10, no. 4, pp. 1297–1301, 2010, doi: 10.1021/nl904092 h.

[12] A. C. Ferrari et al., "Science and technology roadmap for graphene, related two-dimensional crystals, and hybrid systems," *Nanoscale*, vol. 7, no. 11, pp. 4598–4810, 2015, doi: 10.1039/C4NR01600 A.

[13] P. Avouris and C. Dimitrakopoulos, "Graphene: Synthesis and applications," *Mater. Today*, vol. 15, no. 3, pp. 86–97, 2012, doi: 10.1016/S1369-7021(12)70044-5.

[14] M. J. Allen, V. C. Tung, and R. B. Kaner, "Honeycomb carbon: A review of graphene," *Chem. Rev.*, vol. 110, no. 1, pp. 132–145, 2009, doi: 10.1021/cr900070 d.

[15] H. Tian et al., "Graphene dynamic synapse with modulatable plasticity," *Nano Lett.*, vol. 15, no. 12, pp. 8013–8019, 2015, doi: 10.1021/acs.nanolett.5b03283.

[16] M. T. Sharbati et al., "Low-power, electrochemically tunable graphene synapses for neuromorphic computing," *Adv. Mater.*, vol. 30, no. 36, 2018, Art. no. 1802353, doi: 10.1002/adma.201802353.

[17] H. Wang, N. C. Laurenciu, Y. Jiang, and S. D. Cotofana, "Ultracompact, entirely graphene-based nonlinear leaky integrate-and-fire spiking neuron," in *Proc. IEEE Int. Conf. Circuits Syst.*, 2020, pp. 1–5, doi: 10.1109/ISCAS45731.2020.9181092.

[18] V. Pickel and M. Segal, *The Synapse: Structure and Function*. New York, NY, USA: Academic Press, 2013.

[19] S. D. Cotofana, P. Dimitrakis, M. Enachescu, I. Karafyllidis, A. Rubio, and G. C. Sirakoulis, "On graphene nanoribbon-based nanoelectronic circuits viability," in *Proc. 42nd Workshop Compound Semicond. Devices Integr. Circuits Held Eur.*, 2018, pp. 35–36.

[20] R. Sordan, F. Traversi, and V. Russo, "Logic gates with a single graphene transistors," *Appl. Phys. Lett.*, vol. 94, no. 7, 2009, Art. no. 51, doi: 10.1063/1.3079663.

[21] Y. Jiang, N. C. Laurenciu, H. Wang, and S. D. Cotofana, "Graphene nanoribbon based complementary logic gates and circuits," *IEEE Trans. Nanotechnol.*, vol. 18, pp. 287–298, 2019, doi: 10.1109/TNANO.2019.2903480.

[22] G. Liu, S. Ahsan, A. G. Khitun, R. K. Lake, and A. A. Balandin, "Graphene-based non-boolean logic circuits," *J. Appl. Phys.*, vol. 114, no. 15, 2013, Art. no. 154310, doi: 10.1063/1.4824828.

[23] S. Moysidis, I. G. Karafyllidis, and P. Dimitrakis, "Graphene logic gates," *IEEE Trans. Nanotechnol.*, vol. 17, no. 4, pp. 852–859, Jul. 2018, doi: 10.1109/TNANO.2018.2846793.

[24] H. Wang, N. C. Laurenciu, Y. Jiang, and S. D. Cotofana, "Atomistic level hysteresis-aware graphene structures electron transport model," in *Proc. IEEE Int. Symp. Circuits Syst.*, 2019, pp. 1–5, doi: 10.1109/ISCAS.2019.8702106.

[25] A. Morrison, M. Diesmann, and W. Gerstner, "Phenomenological models of synaptic plasticity based on spike timing," *Biol. Cybern.*, vol. 98, pp. 459–478, 2008, doi: 10.1007/s00422-008-0233-1.

[26] U. Jung, Y. J. Kim, Y. Kim, Y. G. Lee, and B. H. Lee, "Extraction of the interface state density of top-gate graphene field-effect transistors," *IEEE Electron Device Lett.*, vol. 36, no. 4, pp. 408–410, Apr. 2015, doi: 10.1109/LED.2015.2402287.

[27] Y. G. Lee et al., "Fast transient charging at the Graphene/SiO_2interface causing hysteretic device characteristics," *Appl. Phys. Lett.*, vol. 98, no. 18, 2011, Art. no. 183508, doi: 10.1063/1.3588033.

[28] C. Huan, Y. Wang, X. Cui, and X. Zhang, "A reconfigurable mixed signal CMOS design for multiple STDP learning rules," in *Proc. IEEE 3rd Int. Conf. Electron. Technol.*, 2020, pp. 639–643, doi: 10.1109/ICET49382.2020.9119574.

[29] C. Mayr et al., "A biological-realtime neuromorphic system in 28 nm CMOS using low-leakage switched capacitor circuits," *IEEE Trans. Biomed. Circuits Syst.*, vol. 10, no. 1, pp. 243–254, Feb. 2016, doi: 10.1109/TBCAS.2014.2379294.

[30] J. Ge et al., "Memristive synapses with high reproducibility for flexible neuromorphic networks based on biological nanocomposites," *Nanoscale*, vol. 12, pp. 720–730, 2020, doi: 10.1039/C9NR08001E.

[31] Z. Wang et al., "Memristors with diffusive dynamics as synaptic emulators for neuromorphic computing," *Nature Mater.*, vol. 16, no. 1, pp. 101–108, 2017, doi: 10.1038/nmat4756.

[32] D. Kaushik, U. Singh, U. Sahu, I. Sreedevi, and D. Bhowmik, "Comparing domain wall synapse with other non volatile memory devices for on-chip learning in analog hardware neural network," *AIP Adv.*, vol. 10, no. 2, 2020, Art. no. 025111, doi: 10.1063/1.5128344.

[33] J. Li et al., "Reproducible ultra thin ferroelectric domain switching for high-performance neuromorphic computing," *Adv. Mater.*, vol. 32, no. 7, 2020, Art. no. 1905764, doi: 10.1002/adma.201905764.

[34] L. F. Abbott and S. B. Nelson, "Synaptic plasticity: Taming the beast," *Nature Neurosci.*, vol. 3, pp. 1178–1183, 2000, doi: 10.1038/81453.

[35] N. Caporale and Y. Dan, "Spike timing-dependent plasticity: A Hebbian learning rule," *Annu. Rev. Neurosci.*, vol. 31, pp. 25–46, 2008, doi: 10.1146/annurev.neuro.31.060407.125639.

[36] S. Datta, *Quantum Transport: Atom to Transistor*. Cambridge, U.K.: Cambridge Univ. Press, 2005.

[37] S. Datta, "Nanoscale device modeling: The Green's function method," *Superlattices Microstructures*, vol. 28, no. 4, pp. 253–278, 2000, doi: 10.1006/spmi.2000.0920.

[38] D. Lee, H. Seo, and W. Jung M., "Neural basis of reinforcement learning and decision making," *Annu. Rev. Neurosci.*, vol. 35, pp. 287–308, 2012, doi: 10.1146/annurev-neuro-062111-150512.

[39] W. Shen, M. Flajolet, P. Greengard, and D. J. Surmeier, "Dichotomous dopaminergic control of striatal synaptic plasticity," *Science*, vol. 321, no. 5890, pp. 848–851, 2008, doi: 10.1126/science.1160575.

[40] C. R. Gerfen and D.J. Surmeier, "Modulation of striatal projection systems by dopamine," *Annu. Rev. Neurosci.*, vol. 34, pp. 441–466, 2011, doi: 10.1146/annurev-neuro-061010-113641.

[41] N. Frémaux and W. Gerstner, "Neuromodulated spike-timing-dependent plasticity, and theory of three-factor learning rules," *Front. Neural Circuits*, vol. 9, no. 85, pp. 1–19, 2015, doi: 10.3389/fncir.2015.00085.

[42] N. Frémaux, H. Sprekeler, and W. Gerstner, "Reinforcement learning using a continuous time actor-critic framework with spiking neurons," *PLoS Comput. Biol.*, vol. 9, no. 4, 2013, Art. no. e1003024, doi: 10.1371/journal.pcbi.1003024.